Numerical and experimental studies on the explosive welding of plates with different initial strength

Xiang-yu Zeng[1] · Xiao-jie Li[1,2] · Xiang Chen[1] · Xiao-hong Wang[1] · Hong-hao Yan[1]

Abstract

In this paper, the effect of initial tensile strength on the explosive welding interface morphology and welding quality was studied. The plates with different initial tensile strength were fabricated via the explosive welding method under the same parameters. Microstructure and hardness at the interface were obtained. According to the characterization, the results demonstrated the morphology of the cross sections is greatly influenced by the strength of the plates. Microhardness analysis confirms that the explosive joining section has work hardening and thermal softening effect occurred. Furthermore, the explosive welding process was numerically simulated by AUTODYN and the temperature distribution of the interfaces was obtained, and it reveals that the strength is negligible and the interface can only be considered as incompressible flow when the pressure ratio $\overline{\sigma}$ is large enough. Otherwise, the strength of the plates cannot be neglected.

Keywords Explosive welding · Material initial strength · Numerical simulation · Wavy interface

1 Introduction

Explosive welding is well known in welding similar or dissimilar metals that cannot be joined by any other techniques [1–4]. Compared with other techniques, a characteristic of explosive welding is that a wavy interface even with vortex always formed instead of a linear interface. A lot of works tried to identify the formation mechanism of the wavy interface. Kowalick [5] recognized that the wavy interface is similar to the Karman vortex streets when the liquid-like interface was disturbed. Bahrani [6] neglected the effect of material strength and considered the wavy interface is formed by the interpenetration of two jet flows. Other authors [7] observed that the Helmholtz instability due to discontinuity in the fluid is similar to the mechanism of interface waves. These studies all considered that the plate is incompressible fluid in the

welding process and ignoring the effect of material initial strength.

Z.M. Zheng [8] studied the explosive welding mechanism by combining theory with metallographic examination; the results indicated that the strength of plates has a great influence on the interface morphology under a low collision velocity. But there are few reports about the influence of the initial strength of welded plates on the interface characteristics. In this study, significant attention is paid to estimate the effect of initial tensile strength on explosive welding in order to better understand how it is affecting the explosive welding. Therefore, the plates with different initial tensile strength were prepared as base plates and welded with a flyer plate under the same explosive welding parameter. The interface morphology and defects were characterized by optical microscopy and SEM. The variation of interface hardness was determined by hardness test. Meanwhile, the explosive welding process was reproduced by numerical simulation to analyze temperature distribution near the welding interface.

✉ Xiao-jie Li
robinli@dlut.edu.cn

1   Department of Engineering Mechanics, Dalian University of Technology, Dalian 116024, People's Republic of China

2   State Key Laboratory of Structural Analysis for Industrial Equipment, Dalian University of Technology, Dalian 116024, People's Republic of China

2 Materials and methods

Figure 1 presents a schematic illustration of the experiment. Four S45C steel plates with the dimensions of $60 \times 40 \times 10$ mm were treated with different tensile strength as the base plates, and a cold rolled Q234 steel plate with the dimension

Fig. 1 Schematic illustration of explosive welding condition
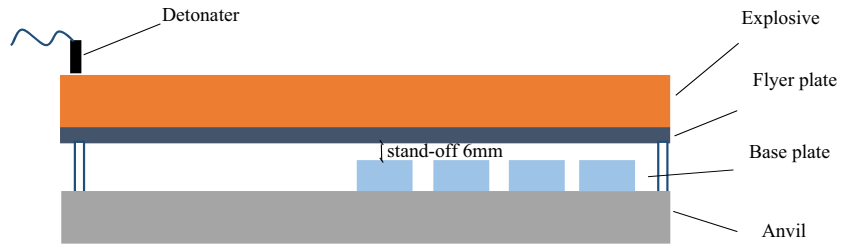
of $400 \times 150 \times 2$ mm was placed parallel to the base plates as the flyer plate. Table 1 shows the chemical compositions of the plates, Table 2 shows the heat treatment processes of the base plates, and Table 3 shows the strength and Vickers hardness of the base plates.

Because of the large span of base plate tensile strength, it is much difficult to select the parameter to weld the four base plates with the same parameter successfully. According to Eq. (1) given by [9–11]:

$$\beta_c = K\sqrt{H_v/\rho V_f^2}, \tag{1}$$

where β_c is the low limit collision angle of "re-entry jet"; K is determined by the degree of surface finish of the plates; H_v is the Vickers hardness; and ρ is the density. When the flyer plate is parallel to the base plate, V_f is equal to the detonation velocity of explosive V_d. And,

$$V_p = 2V_d \sin(\beta/2), \tag{2}$$

then,

$$K\sqrt{H_v/\rho} = \frac{\beta_c}{2\sin(\beta_c/2)}V_p, \tag{3}$$

in explosive welding, the collision angle $\beta_c \approx 5\sim25°$, so $\beta_c \approx 2\sin(\beta_c/2)$, then,

$$V_{pmin} = K\sqrt{H_v/\rho}. \tag{4}$$

According to Eq. (4), in order to weld all the base plates successfully, the terminal flyer velocity was selected as about 700 m/s. In this experiment, the ANFO explosive with the density of 0.99 g/cm³ was chosen with the thickness of 30 mm, and the velocity of which was 2311 m/s measured by a continuous velocity probe as shown in Fig. 2 [12]. The collision velocity V_p was 744 m/s when the collision angle β was 18° according to Eq. (2) The standoff distances were calculated by the program of the material point method [13]; as a result, 6 mm was used.

The explosive welding specimens were cut at the place 45~50 mm from the detonation point where stable wave interface was formed, and the cutting direction parallel to the detonation direction. Then, the specimens were polished using 240, 400, 800, and 1500 grit waterproof SiC paper. Finally, the polishing was finished using a cloth and diamond paste. After polishing, 4% nitric acid alcohol solution was used to etch the specimens. The morphologies of the specimens were characterized by optical microscopy using a Carl Zeiss Axio Observer Z1m metallographic microscopy and SEM(Quanta 450), and the hardness was measured via a HVS-1000S Vickers hardness tester.

3 Numerical simulation

The simulation of explosive welding was carried out by the smoothed particles hydrodynamics (SPH) method combined with the finite element method. This method not only guarantees the accuracy of calculation but also improves the computational efficiency. The SPH method has obvious advantages in dealing with large deformations and moving discontinuities such as high-velocity impact welding even accompany with metal jets formed. The conservation equation of particle motion is given as:

$$\prod^h f(x) = \int_{-2h}^{2h} f(y)W(x-y,h)dy, \tag{5}$$

where x and y are the spatial locations of the interest particle, and its neighboring particles within the smooth length h from it. The entire SPH model was dynamically divided into several zones with a radius of $2h$ to control the number of particles in each region. By this way, the computational efficiency was improved under the permission of the accuracy of the calculation [11]. W is the Kernel function. The SPH particles with density increased were placed on the inner side of the plates, besides that the flyer plate was filled with sparse particles and the base plate was used a finite element grid. Adiabatic model was used because the

Table 1 Chemical composition of experiment materials (%)

Materials	C	Ni	Cr	Fe	Mn	P	Si	S
S45C	0.5	0.25	0.25	Rest	0.6	0.035	0.3	–
Q235	0.2	–	–	Rest	0.6	0.045	0.3	0.05

Table 2 Heat treatment of the 1045 steel

Base plates	NO.1	NO.2	NO.3	NO.4
Heat treatment	Tempering	Tempering	Tempering	Tempering
Temp., °C	550	500	400	200
Time, min	30	40	50	60

Table 3   Tensile strength of the base plates

Base plate	NO.1	NO.2	NO.3	NO.4
Tensile strength/MPa	357	895	1529	2588
Vickers hardness	105	268	449	760

interface waves only formed and developed within a few wavelengths behind the collision point in explosive welding; therefore, the result of adiabatic model is similar to heat conduction model in this space scale [14].

The simulation was carried out by using Ansys AUTODYN; the model of numerical simulation is shown in Fig. 3. According to the experimental data, the flyer plate was rotated 18° and a speed of 744 m/s was applied on the flyer plate. The plates were treated as Johnson-Cook type plastic materials, and the Mie-Gruneisen equation of state was used to calculate the temperature distribution. The parameters of the flyer plate are shown in Table 4. The influence of strength of the base plate on explosive welding was studied.

4 Results and discussions

4.1 Effect of strength pressure ratio $\overline{\sigma}$

The interface optical micrograph of the four groups of the explosive welding specimens are presented in Figs. 4, 5, 6, and 7, and Table 5 shows the statistics of the amplitude and wavelength. The typical wave interface can be seen in all the specimens. However, due to the various strengths of the base plates, the morphology and the dimension of the interface are different obviously. The wave amplitude and wavelength can be used to estimate the state of the plates in the welding process. According to Eq. (6),

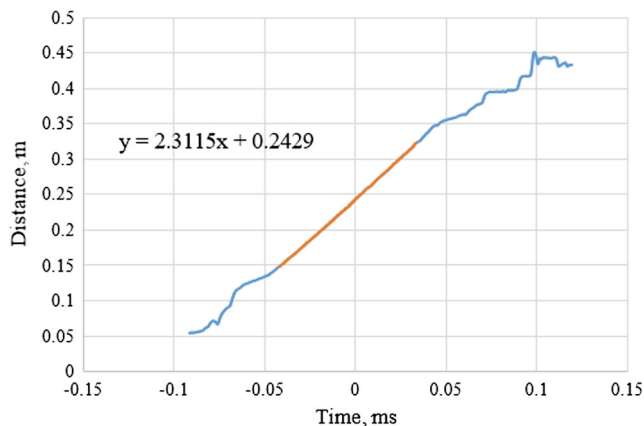$$\overline{\sigma} = \sigma/p \tag{6}$$

$$p = \frac{1}{2}\rho_f V_f^2 \tag{7}$$
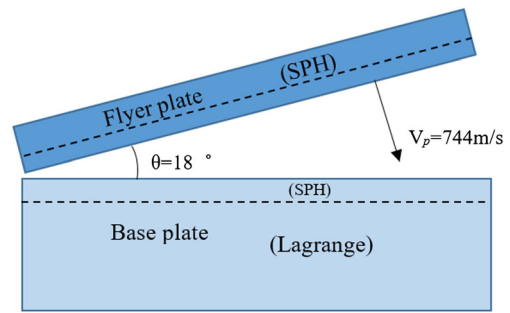

Fig. 2   The determination of explosive velocity

Fig. 3   The model of explosive welding in the simulation

where $\overline{\sigma}$ is the pressure ratio and σ is the strength of plates; p is the dynamic pressure of the collision point, which can be calculated by Eq. (7). The pressure ratio $\overline{\sigma}$ of specimen NO.1 is nearly 228, which is much higher than those of the other specimens (91 of NO.2; 52 of NO.3; 31 of NO.4). In this case, the material strength is negligible and the interface can be considered as incompressible flow [15, 16], which caused large molten region to form on the interface and made the wave interface hard to measure.

To the other three specimens with higher strength and lower $\overline{\sigma}$ than specimen NO.1, there is no continuous molten region formed on the interface. The largest amplitude and the shortest wavelength formed on the interface of specimen NO.2, and the amplitude decrease while the wavelength rise from specimen NO.2 to NO.3, which can be concluded by Bahrani mechanism [8] that the flyer plate penetrates deeper pits on the base plate with lower strength; this pit blocks the growth of the wavelength. When the strength of the base plate exceeds specimen NO.3, the wavelength appears a significant downward trend, which indicates that the strength of the plate inhibits the growth of interface waves. In this case, the cross section cannot be treated as flow and ignore the strength.

4.2 Interfacial Microstructures

The amplitude and wavelength of the interface wave cannot be measured accurately in specimen NO.1 as shown in Fig. 4(a),; instead, continuous as-cast structure formed on the interface as shown in Fig. 4(b). The molten regions were attributed to the adiabatic heating [17]. Due to the low strength, the shear strain on the interface was larger, which makes more strain energy converted into thermal energy than other specimens with higher strength.

As the initial strength of the base plate increased to 895 MPa, the over-melted phenomenon is obviously relieved. Figure 5(a) shows that only a small amount of as-cast structure can be observed at the crest of the base plate. Under this condition, the obvious wave interface formed. The grains near the wavy interface is obviously elongated under the effect of crimping and punching shear. A small amount of the jet cannot escape and be wrapped in the vortex of the wave and

Table 4 The parameters of the flyer plate

Material	Shear modulus/ GPa	Yield stress/ GPa	Hardening constant/ GPa	Hardening exponent	Strain rate constant	Thermal softening exponent	Melting temperature	Ref. strain rate/s
Q235	77.3	0.325	0.220	0.16	0.015	1.03	1795	1.16

formed as-cast structure as shown in Fig. 5(b), eventually. These residual jets declined the cleaning effect on the interface and may have affected the bonding strength.

With the initial tensile strength of the base plates increased to 1592 MPa, the plastic deformation is decreased gradually as displayed in Fig. 6. The periodic waves are formed at the interface. The crest of the base plate interface wave is sheared into an "isolated island" by a continuous band as indicated by the arrow in Fig. 6(b). It can be concluded that the plate is softened by thermal generated from the severe plastic deformation and sheared by flyer plate.

As illustrated in Fig. 7, NO.4 specimen shows an inapparent wavy morphology compared with other specimens. In addition, no apparent molten region and "isolated island" formed on the interface. The cracks and adiabatic shear bands (ASBs) is observed in the NO.4 specimen, as indicated in Fig. 7(a, b). The shear bands with an angle of about 45° appear on the base plate along the interface. The cracks only appeared on the base plate side with the direction parallel to the interface wave tangent; it reveals shear stress concentrated in these places. No adiabatic shear band and crack are observed on the flyer plate. The severe plastic deformation under high strain rate induces the dramatic temperature rise near the interface, which leads to the flow stress decreased and localized plastic instability, and eventually formed ASBs [18].

4.3 SEM analysis of interfaces

To achieve high-resolution images, the interfaces of the specimens were tested by SEM.

Figure 8 presents the SEM images of NO.1 specimen. It can be seen from Fig. 8(a) that hollow pores and cracks appeared in the molten region. The diameters of the pores are larger in the center of the as-cast structure and smaller in the edge. The dendritic structures are observed around the as-cast structure as shown in Fig. 8(b). Under the explosive welding conditions with a 2296 m/s detonation velocity, the gas between the two plates is drawn and enclosed in the molten

vortex, which formed the hollow pores. The high cooling rate during the solidification process creates interior stress in the molten region, which leads to the formation of cracks [1].

The shear bands and cracks can be observed on the base plates of NO.3 and NO.4 specimens as shown in Fig. 9(a, b), respectively. No shear bands or cracks were observed on flyer plates. The shear band cut through the vortex and formed the "inland area" as presented in Fig. 9(a). The adiabatic shear bands and cracks can be observed along the interface in NO.4 specimen as shown in Fig. 9(b). Once the cracks are generated, they are free to grow in the plate even parallel to the interface. Experienced the dramatic temperature rise and high cooling rate process, the grains in shear bands are defined and formed fine equiaxed grains resulting from dynamic recrystallization [18]; consequently, the hardness and strength of the bands are increased enough to shear the plate.

4.4 Interface hardness distribution

The hardness of the interfaces was made under an indenter load of 150 g. The indentations were located 300 μm from each other to allow the smaller distance intervals from the bond line and each indentation not affect each other. The hardness values of interface profile are shown in Fig. 10.

The flyer plate far from the interface had a microhardness of 150 HV, and with the distance decrease from the interface, the hardness of all flyer plates increased by work hardening effect. The work hardening effect has various degree of influences on the flyer plates; the higher initial strength formed, the stronger the hardening effect. On the other hand, the microhardness on the base plates decreased far from the interface. The work hardening effect is mainly owing to grain refinement and plastic deformation [19, 20]. The decrease of the hardness in the base plates is mainly due to the softening effect caused by the temperature rise, and the softening effect has greater influence on hardness compared with the work hardening in the case of explosive welding high strength plates [21].

Fig. 4 Microscopy images of the cross section of specimen NO.1 (**a**) interface, (**b**) high-resolution image of position b in (**a**)
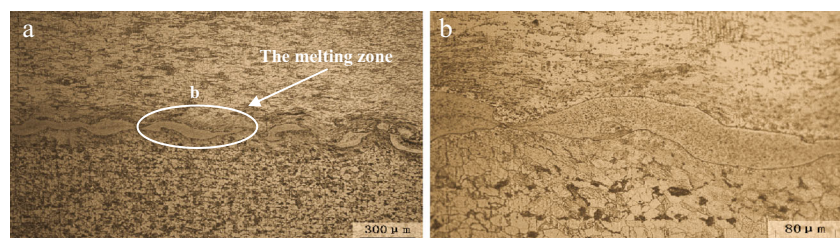
Fig. 5 Microscopy images of the cross section of specimen NO.2 (**a**) interface, (**b**) high-resolution image of position b in (**a**), (**c**) high-resolution image of position c in (**b**), (**d**) high-resolution image of position d in (**b**)
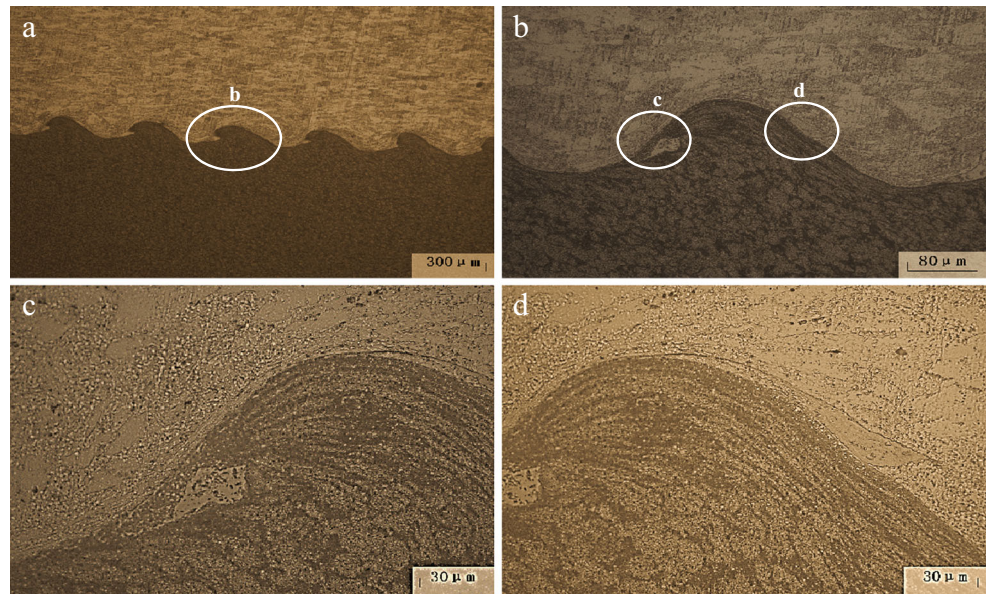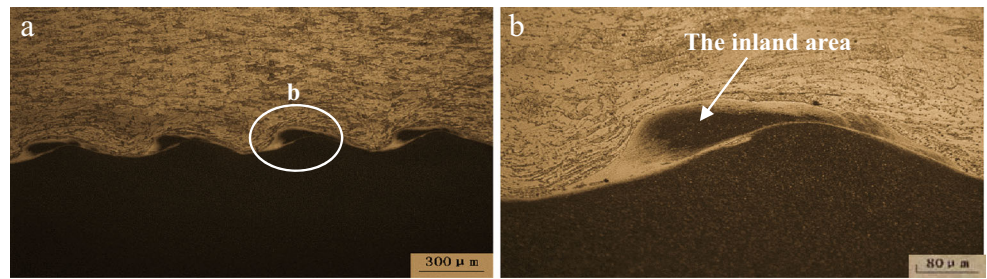

Fig. 6 Microscopy images of the cross section of specimen NO.3 (**a**) interface, (**b**) high-resolution image of position b in (**a**)

Table 5 Interface wave parameters of each welding specimen

Specimen Parameter (μm)	NO.1	NO.2	NO.3	NO.4
Amplitude	–	180.2	148.8	70.0
Wavelength	–	396.8	567.5	402.5

Fig. 7 Microscopy images of the cross section of specimen NO.4 (a) interface, (b) high-resolution image of position b in (a)
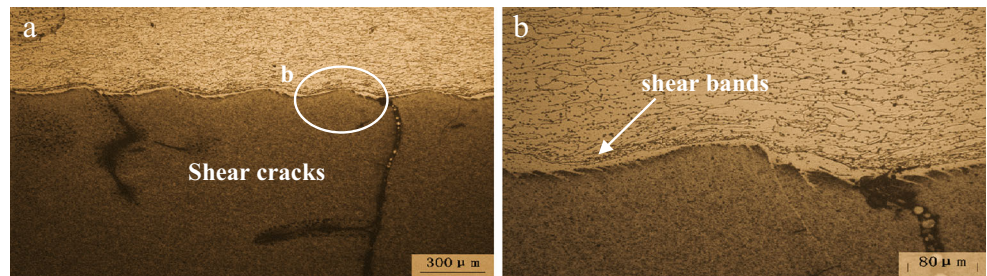
Fig. 8 SEM images of the NO.1 specimen. (**a**) hollow pores and cracks, (**b**) dendritic structures
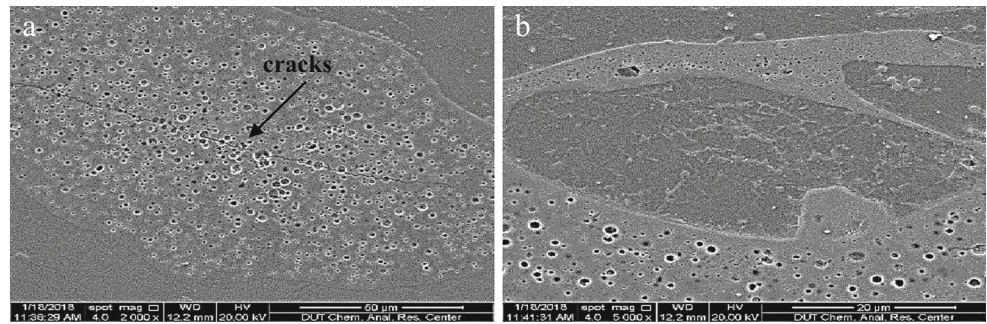

Fig. 9 SEM images of cross section (**a**) shear band of NO.3 specimen, (**b**) adiabatic shear bands and cracks of NO.4 specimen
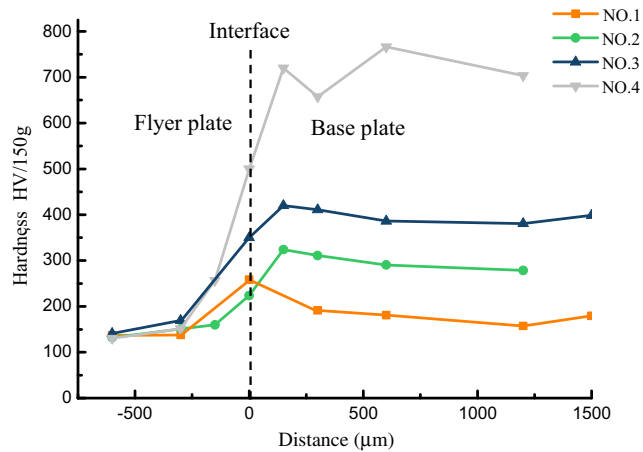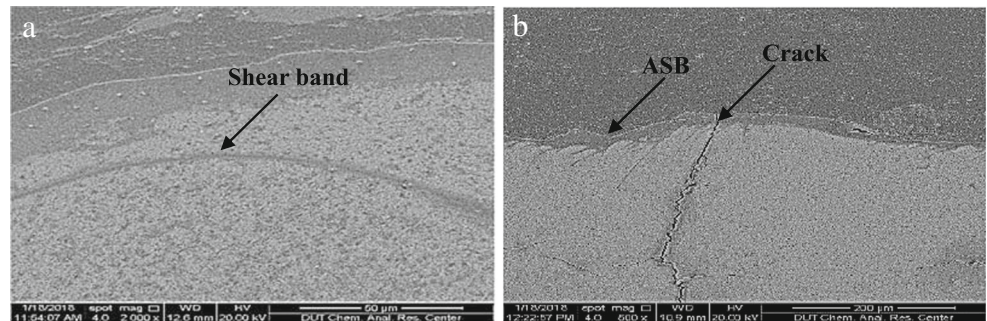

Fig. 10 Microhardness distribution at the interface of the four specimens

Fig. 11 The numerical simulation interface morphology, (**a**) NO.1 specimen, (**b**) NO.2 specimen, (**c**) NO.3 specimen, (**d**) NO.4 specimen
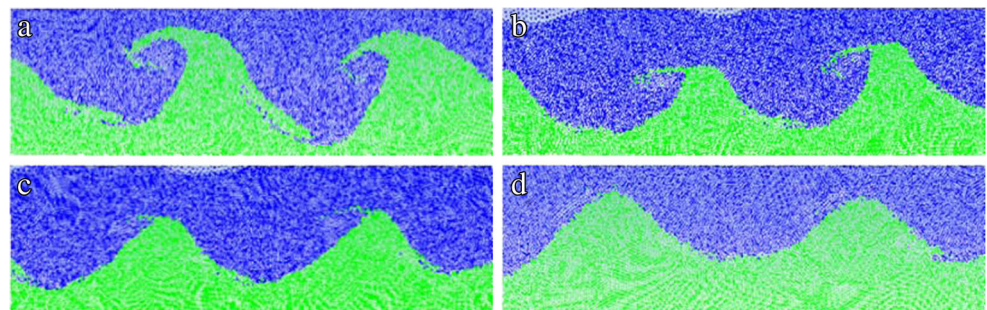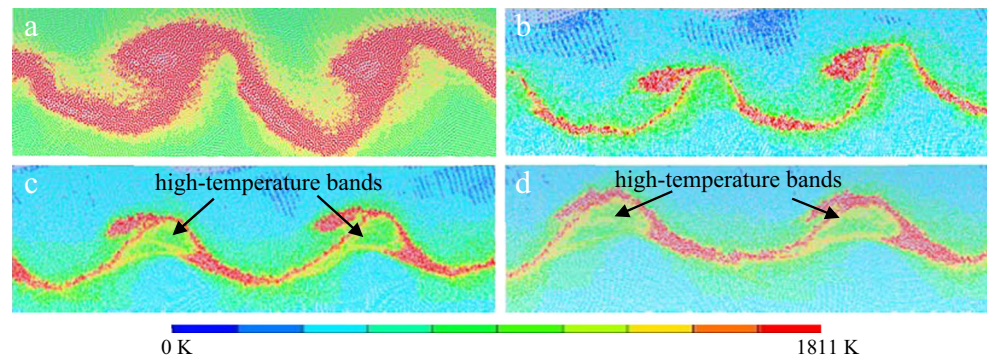
Fig. 12 Distributions of temperature at interface (**a**) NO.1 specimen, (**b**) NO.2 specimen, (**c**) NO.3 specimen, (**d**) NO.4 specimen

4.5 Numerical simulation

Figure 11 presents the simulation results of the interface morphology of all specimens. Comparing with the interface morphology in Figs. 4, 5, 6, and 7, the numerical simulation results are close to the experimental results. It demonstrates that the model and the material parameters are in line with the experiment and could be used in numerical simulation.

The distributions of temperature are shown in Fig. 12. Molten region formed in all the specimens during the welding process, which makes the metal jet clean the surface. The NO.1 specimen shows a larger high temperature and molten region as displayed in Fig. 12(a). Under the same explosive welding condition, the flyer plate oblique collision, the base plates with the same velocity, the plates with lower initial strength will generate larger plastic deformation, which induces more thermal generated and accumulated on the interface and formed as-cast structure.

High-temperature bands can be observed as indicated with arrows in Fig. 12(c, d), and the site was the same with the adiabatic shear bands as shown in Figs. 6 and 7. These bands are always observed in the materials with higher initial strength, which can be concluded as follows:

$$dT = \frac{du}{C_v} = \frac{\sigma.d\varepsilon}{C_v}, \tag{8}$$

$$\sigma\left(\varepsilon.\dot{\varepsilon}.T\right) = C_v\frac{dT}{d\varepsilon}, \tag{9}$$

$$\begin{cases} \dfrac{d\sigma}{d\varepsilon} > 0 \to \dfrac{d^2T}{d\varepsilon^2} > 0 \\ \dfrac{d\sigma}{d\varepsilon} < 0 \to \dfrac{\mathrm{d}^2T}{d\varepsilon^2} < 0 \end{cases}, \tag{10}$$

where T is the temperature, u is the internal energy generated by the oblique collision, C_v is the specific heat capacity, σ is the stress; ε is the strain, and $\dot{\varepsilon}$ is the strain rate. According to Eq. (10), the materials with higher initial strength have a longer period before strength failure ($\frac{d\sigma}{d\varepsilon} > 0$) and longer temperature-accelerated period ($\frac{d^2T}{d\varepsilon^2} > 0$). The longer temperature-accelerated period leads to the temperature rising more sharply, and the plates are subjected to greater pressure when thermal softening occurs. Because of these results, the adiabatic shear bands and cracks are always generated in the materials with higher initial strength.

5 Conclusions

The effect of the initial strength of the base plates on explosive welding was studied in this paper. The conclusions are as follows:

1. The interface morphology of explosive welding is strongly affected by the strength of the plates. The interface transforms from the continuous as-cast structure interface to wave interface and finally to the nearly linear interface with the strength of the plates increase.
2. The strength is negligible and the interface can be considered as incompressible flow when the pressure ratio $\overline{\sigma}$ is large. Otherwise, the strength of the plates cannot be neglected or considered as flow.
3. Continuous as-cast structure filled with pores formed accompanied with cracks is observed in the molten region of the plate with lower strength, which means the plates with lower strength will undergo greater plastic strain and generate more thermal during welding, and the defects like cracks always form in the as-cast structure.
4. The shear bands were observed in the plates with high strength, which can even cut the vortex into "isolated island" and formed cracks, which is due to the temperature rising faster in the plates with higher strength, and the plates are subjected to greater pressure when thermal softening occurs.
5. Work hardening effect could be seen on the interface of all the specimens, which is mainly due to plastic deformation during the welding process. The decrease of hardness is also observed at the base plates with higher initial strength, and it is mainly due to heat softening effect.

References

1. Bataev IA, Lazurenko DV, Tanaka S, Hokamoto K, Bataev AA, Guo Y, Jorge AM Jr (2017) High cooling rates and metastable phases at the interfaces of explosively welded materials. Acta Mater 135:277–289. https://doi.org/10.1016/j.actamat.2017.06.038

2. Liu C, Shanthraj P, Diehl M, Roters F, Dong S, Dong J, Ding W, Raabe D (2018) An integrated crystal plasticity–phase field model for spatially resolved twin nucleation, propagation, and growth in hexagonal materials. Int J Plast 106:203–227. https://doi.org/10.1016/j.ijplas.2018.03.009

3. Paul H, Morgiel J, Baudin T, Brisset F, Prażmowski M, Miszczyk M (2014) Characterization of explosive weld joints by TEM and SEM/EBSD. Arch Metall Mater 59:1129–1136. https://doi.org/10.2478/amm-2014-0197

4. Mali VI, Bataev AA, Maliutina IN, Kurguzov VD, Bataev IA, Esikov MA, Lozhkin VS (2017) Microstructure and mechanical properties of Ti/Ta/Cu/Ni alloy laminate composite materials produced by explosive welding. Int J Adv Manuf Technol 93:1–10. https://doi.org/10.1007/s00170-017-0887-8

5. Vigueras D (2007) Explosive and impact welding: technical review. Mater Technol 22:200–204. https://doi.org/10.1179/175355507X236740

6. Bahrani AS, Black TJ, Crossland B (1967) The mechanics of wave formation in explosive welding. Proc R Soc A: Mathematical, Physical and Engineering Sciences 296:123–136. https://doi.org/10.1098/rspa.1967.0010

7. Reid SR (1978) Wake instability mechanism for wave formation in explosive welding. Int J Mech Sci 20:247–253. https://doi.org/10.1016/0020-7403(78)90086-3

8. Chemin C, Qingming T (1989) Mechanism of wave formation at the interface in explosive welding. Acta Mech Sinica 5:97–108. https://doi.org/10.1007/BF02489134

9. Aizawa Y, Nishiwaki J, Harada Y, Muraishi S, Kumai S (2016) Experimental and numerical analysis of the formation behavior of intermediate layers at explosive welded Al/Fe joint interfaces. J Manuf Process 24:100–106. https://doi.org/10.1016/j.jmapro.2016.08.002

10. Ribeiro JB, Mendes R, Loureiro A (2014) Review of the weldability window concept and equations for explosive welding. J Phys Conf Ser 500:38. https://doi.org/10.1088/1742-6596/500/5/052038

11. Zhou Q, Feng J, Chen P (2017) Numerical and experimental studies on the explosive welding of tungsten foil to copper. Materials 10: E984. https://doi.org/10.3390/ma10090984

12. Li K, Li X, Yan H, Wang X, Wang Y (2018) Study of continuous velocity probe method for the determination of the detonation pressure of commercial explosives. J Energ Mater 00:1–9. https://doi.org/10.1080/07370652.2018.1425310

13. Wang Y, Beom HG, Sun M, Lin S (2011) Numerical simulation of explosive welding using the material point method. Int J Impact Eng 38:51–60. https://doi.org/10.1016/j.ijimpeng.2010.08.003

14. Li XJ, Mo F, Wang XH, Wang B, Liu KX (2012) Numerical study on mechanism of explosive welding. Sci Technol Weld Join 17:36–41. https://doi.org/10.1179/1362171811Y.0000000071

15. Sun W, Li XJ, Hokamoto K (2013) Numerical simulation of underwater explosive welding process. Mater Sci Forum 767:120–125. https://doi.org/10.4028/www.scientific.net/MSF.767.120

16. Akbari M, Saedodin S, Toghraie D, Shoja-Razavi R, Kowsari F (2014) Experimental and numerical investigation of temperature distribution and melt pool geometry during pulsed laser welding of Ti6Al4V alloy. Opt Laser Technol 59:52–59. https://doi.org/10.1016/j.optlastec.2013.12.009

17. Akbari Mousavi SAA, Farhadi Sartangi P (2009) Experimental investigation of explosive welding of cp-titanium/AISI 304 stainless steel. Mater Des 30:459–468. https://doi.org/10.1016/j.matdes.2008.06.016

18. Yan YB, Zhang ZW, Shen W, Wang JH, Zhang LK, Chin BA (2010) Microstructure and properties of magnesium AZ31B-aluminum 7075 explosively welded composite plate. Mater Sci Eng A 527:2241–2245. https://doi.org/10.1016/j.msea.2009.12.007

19. Jinlong L, Tongxiang L, Limin D, Chen W (2016) Influence of sensitization on microstructure and passive property of AISI 2205 duplex stainless steel. Corros Sci 104:144–151. https://doi.org/10.1016/j.corsci.2015.12.005

20. Mohammed G, Ishak M, Aqida S, Abdulhadi H (2017) Effects of heat input on microstructure, corrosion and mechanical characteristics of welded austenitic and duplex stainless steels: a review. Metals 7:39. https://doi.org/10.3390/met7020039

21. Sun W, Li X, Yan H, Hokamoto K (2014) Effect of initial hardness on interfacial features in underwater explosive welding of tool steel SKS3. J Mater Eng Perform 23:421–428. https://doi.org/10.1007/s11665-013-0778-6

Publisher's note Springer Nature remains neutral with regard to jurisdictional claims in published maps and institutional affiliations.